Journal of the Physical Society of Japan
Vol. 69, No. 6, June, 2000, pp. 1895-1906

Interplay between Raman and Fluorescence-Like Components in Resonant X-ray Emission Spectra of Degenerate d^0 and d^1 Systems

Tsuyoshi IDÉ* and Akio KOTANI

Institute for Solid State Physics, The University of Tokyo, 5-1-5 Kashiwanoha, Kashiwa, Chiba 277-8581

(Received February 10, 2000)

Resonant X-ray emission spectra (RXES) are theoretically studied with a doubly-degenerate one-dimensional periodic Anderson model under d^0 and d^1 fillings, together with normal X-ray emission spectra (NXES) and X-ray absorption spectra (XAS). The model is regarded as a simplified model of band insulators such as TiO_2, and Mott-Hubbard insulators such as Ti_2O_3. Comparing with nondegenerate model calculations, we point out the important role of orbital degeneracy in reproducing experimental excitation energy dependence of RXES. The calculated results exhibit interplay between Raman and fluorescence-like components in both band insulator and Mott-Hubbard insulator. The former and latter components reflect the local point symmetry and the translational symmetry of the system, respectively. Our results qualitatively well explain Ti $3d$-$2p$ RXES of TiO_2 and Ti_2O_3.

KEYWORDS: resonant X-ray emission, incident energy dependence, orbital degenedacy, periodic Anderson model, Mott-Hubbard insulator, fluorescence-like component, Lanczos method

§1. Introduction

Since the advent of the third-generation synchrotron light sources, resonant X-ray emission spectroscopy (RXES) has been attracted much attention in material science. RXES is a coherent second-order optical process, where an incident X-ray photoexcites a core electron to an absorption threshold, and then a valence electron radiatively decays to bury the core hole. The second order perturbation theory with respect to electron-photon interaction shows that the spectral function of RXES obeys the selection rule of a local point group and as well as the translational group of the whole crystal. This feature is especially suitable to study electronic structures of strongly-correlated $3d$ systems, where one may be interested in the duality between localized and itinerant behavior of $3d$ electrons.

In 1996, Tezuka *et al.* reported strange dependence on excitation energy (Ω) in Ti $3d$-$2p$ RXES of TiO_2.[1] Their data show two series of inelastic spectra: One is those spectra whose emitted photon energy (ω) is linearly shifted as increasing Ω. In the other, however, ω is nearly independent of Ω, and is smoothly connected with the peak of "normal" X-ray emission spectra. We call the former series of spectra "Raman component", and the latter "fluorescence-like component" hereafter.

The normal X-ray emission spectroscopy (NXES) is also the coherent second-order optical process, where an incident X-ray photoexcites a core electron to a high-energy continuum (Fig. 1(a)). Despite the apparent resemblance, NXES is quite different from RXES in at least two respects. First, since the photoexcited electron simply acts as a spectator one towards the valence system, ω is independent of Ω in principle; ω roughly reflects DOS of the filled valence band. Some authors call NXES spectra "fluorescence" by this reason. Second, apart from the photoelectron, the number of electrons in the final state decreases by one from that of the initial state. Therefore, it is a puzzle for us to observe the fluorescence-like component in RXES spectra. Interestingly, the fluorescence-like component is absent in experimental Ti $3d$-$2p$ RXES spectra of gas-phase $TiCl_4$,[2] which is composed of molecules with nominally d^0 configuration. This is the evidence that the fluorescence-like component originates from the solid state effect, possibly due to the itinerancy of a $3d$ electron itself.

The intermediate state of RXES is the same as the final state of X-ray absorption spectroscopy (XAS). It has been established that the experimental XAS as well as X-ray photoemission spectroscopy (XPS) spectrum of TiO_2 is well reproduced with a TiO_6 cluster model including *both* core-$3d$ and $3d$-$3d$ correlation *explicitly*.[3] Accordingly, one may expect that a dominant class of intermediate state, when Ω is tuned at the absorption threshold, is fairly localized in a photoexcited TiO_6 unit, and that final states left after an X-ray emission process from these intermediate states should be described within local CT excitations, being strongly dependent on the nature of the intermediate states. As far as one confines oneself to the cluster model, the energy conservation rule

$$\omega = E_g - E_f + \Omega,$$

never predicts the fluorescence-like spectra over whole range of the absorption threshold; It rather predicts the existence of the Raman component. Here E_g and E_f are electronic energies of the ground state and a final state, respectively.

* Present address: IBM Tokyo Research Laboratory, 1623-14 Shimotsurumae, Yamato-shi. E-mail: e30591@jp.ibm.com

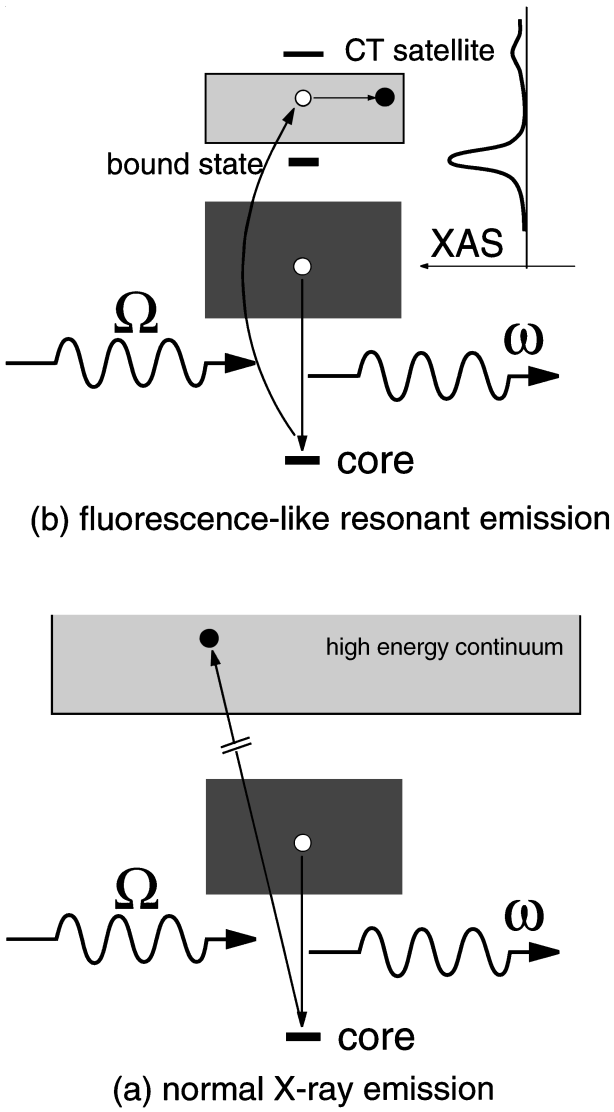

Fig. 1. Schematic diagram of (a) the normal X-ray emission process and (b) the fluorescence-like resonant emission in M 3d-2p RXES of d^0 compounds. In (a), a core electron is excited by an incident X-ray with energy Ω to a high-energy continuum far from the valence level, so that the spectrum of the emitted X-ray ω is related to the density of states of the filled valence band (darkly-shaded area). In (b), a core electron is resonantly excited to an extended valence state located between the main and CT satellite peaks of XAS. Then the electron escapes from the core hole site, with probability involving 3d-ligand hopping integral and relaxation time $\tau_{\rm R}$ of the intermediate state. After that, the X-ray emission process resembles the case (a).

In this paper, we discuss M 3d-2p RXES (M being a transition metal ion) for d^0 and d^1 insulators with multi-M cluster models including *orbital degeneracy*. We have proposed a mechanism of electronic origin in the previous paper[4] for the fluorescence-like spectra. The key point of our picture is the existence of extended states *against* the strong core hole potential in the intermediate state, although such extended states may have almost negligible weight in the XAS spectrum. When Ω is tuned there, an electron excited to a 3d orbital can escape to the neighboring sites (Fig. 1(b)) because of a finite band width. Consequently, RXES spectra roughly reflect the density of states of the valence system. This transition process resembles NXES in the sense that a core electron is excited to a continuum state in the both cases. Thus, one can call this RXES spectrum NXES-like one, which has naturally less Ω-dependence.

While our model successfully explained the origin of the fluorescence-like spectra, the lack of internal structure of atoms prevents us from discussing features of local origin such as polarization dependence in RXES. Very recently, Harada *et al.* observed polarization dependence of Ti 3d-2p RXES of TiO_2, where drastic resonant enhancement occurs when Ω is tuned at a satellite peak of XAS,[5] and Matsubara *et al.* pointed out that it is explained in terms of the selection rule of the local point group.[6] It is a purpose of the present paper to extend the previous model to include orbital degeneracies, and show that calculated spectra represent coexistence of the fluorescence-like and Raman components, the latter being qualitatively consistent to the experimental polarization dependence.

Another purpose of the present paper is to study the RXES in a Mott-Hubbard insulator. If an inter-site charge-transfer process crucially contributes to RXES spectra in the appearance of the fluorescence-like component, it is interesting to study how RXES spectra are suffered from change in character of insulating gaps upon going from a band insulator to a MH insulator. Although effective hopping energy seems to be considerably reduced by d-d on-site Coulomb interaction, experimental data on Ti 3d-2p RXES of Ti_2O_3,[7] which is often referred to as a typical MH insulator, show a clear fluorescence-like component. In the subsequent sections, we show that orbital degeneracy is essential in the appearance of the fluorescence-like spectra in MH systems, and we sketch interplay between the fluorescence-like component and intra- or inter-site d-d excitations in RXES spectra.

The layout of the present paper is as follows: In the next section, the models used are explained. As a minimal model with both translational symmetry and orbital degeneracies, a doubly-degenerate one-dimensional (1D) model is introduced. In §3 and 4, main features of calculated results are discussed in detail for d^0 and d^1 systems, respectively, with special attention to the role of orbital degeneracy and translational symmetry of the system. In §5, the aforementioned coexistence and relation with experimental data are discussed. In §6, a brief summary is given.

§2. Formulation

2.1 Hamiltonian

We use a 1D doubly-degenerate periodic Anderson model, which is topologically equivalent to the system schematically described in Fig. 2(a). The Hamiltonian is written as follows:

$$H = H_0 + V + H_{dd} + H_{dc}, \tag{2.1}$$

where the first two terms describe one-electron part, the third one 3d-3d Coulomb interaction, and the forth one 3d-core intra-atomic Coulomb interaction.

H_0 and V are defined as

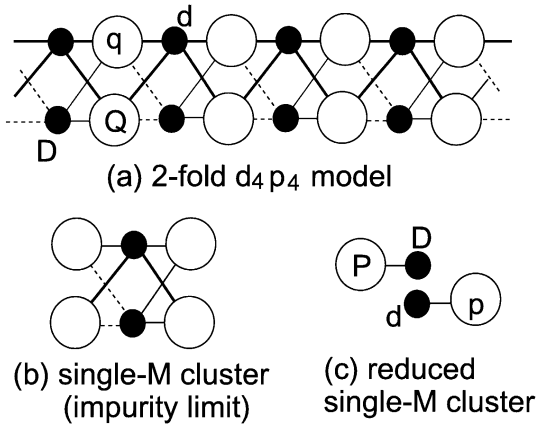

Fig. 2. The *degenerate d-p* models used. (a) A topologically equivalent system of the doubly degenerate periodic d_4p_4 model. (b) The single-M cluster model with *open* boundary condition. (c) The reduced single-M cluster model, where d-D Coulomb interaction couples the two subsystems. For the definition of the orbitals P and p, see the text. In these figures, the black and white circles represent Ti $3d$ and oxygen $2p$ orbitals, respectively. The d-p transfer with positive sign is described with the solid lines, whereas transfer with negative sign is described with dashed lines. Note that local symmetries around the nonequivalent $3d$ orbitals (d and D) are not the same.

$$H_0 = \sum_{l,\sigma}[\varepsilon_0\, Q^\dagger_{l\sigma}Q_{l\sigma} + \varepsilon_0\, q^\dagger_{l\sigma}q_{l\sigma} + \varepsilon_c\, c^\dagger_{l\sigma}c_{l\sigma} + (\Delta+\varepsilon_0)\, D^\dagger_{l\sigma}D_{l\sigma} + (\Delta - 10Dq + \varepsilon_0)\, d^\dagger_{l\sigma}d_{l\sigma}],$$

$$V = \sum_{l,\sigma}\{d^\dagger_{l\sigma}[v_1(q_{l\sigma}+q_{l+1\sigma}) + u_1(Q_{l\sigma}+Q_{l+1\sigma})] + D^\dagger_{l\sigma}[v_2(Q_{l\sigma}-Q_{l+1\sigma}) + u_2(q_{l\sigma}-q_{l+1\sigma})]\} + \text{H.c.}$$

In the above equations, $d^\dagger_{l\sigma}$ and $D^\dagger_{l\sigma}$ represent creation operators of two $3d$ orbitals with spin σ at l-th unit cell, respectively. $q^\dagger_{l\sigma}$ and $Q^\dagger_{l\sigma}$ are creation operators of oxygen $2p$ orbitals with one-electron energy ε_0. Δ and $10Dq$ are the CT energy and the crystal field splitting energy between the two $3d$ orbitals. $c^\dagger_{l\sigma}$ is a creation operator of a core electron with one-electron energy ε_c.

The interaction terms are defined as

$$H_{dd} = U_{d1}\sum_l (d^\dagger_{l\uparrow}d_{l\uparrow}d^\dagger_{l\downarrow}d_{l\downarrow} + D^\dagger_{l\uparrow}D_{l\uparrow}D^\dagger_{l\downarrow}D_{l\downarrow}) + U_{d2}\sum_l \left(\sum_\sigma d^\dagger_{l\sigma}d_{l\sigma}\right)\left(\sum_{\sigma'} D^\dagger_{l\sigma'}D_{l\sigma'}\right)$$

and

$$H_{dc} = -U_{dc}\sum_{l,\sigma,\sigma'}\left(d^\dagger_{l\sigma}d_{l\sigma} + D^\dagger_{l\sigma}D_{l\sigma}\right)c_{l\sigma'}c^\dagger_{l\sigma'}, \qquad (2.2)$$

where U_{d1} (U_{d2}) is the on-site d-d or D-D (d-D) Coulomb correlation energy, and U_{dc} is the intra-atomic core-$3d$ interaction. Exchange and spin-orbit couplings are omitted for simplicity. Note that our model explicitly contains both U_{dd} and U_{dc}, which are essential to have realistic discussion on XAS,[3] and therefore RXES.

The d-p hopping energies are represented with $\{v_1, v_2, u_1, u_2\}$. Depending on their relative phases and values, there are some ways to include orbital degeneracy into this model. The single-metal-ion cluster limit of our model is described in Fig. 2(b). We consider that the single-M cluster is an effective model of an MO_6 cluster. In the case of an MO_6 cluster with O_h symmetry, a subsystem having $d(e_g)$ orbitals and ligand orbitals with e_g symmetry is coupled with a subsystem having $d(t_{2g})$ orbitals and ligand orbitals with t_{2g} symmetry through d-d Coulomb interaction. If there were no Coulomb interaction, the subsystems would be completely decoupled. Considering this fact, we set $v_1 = u_1$ and $v_2 = u_2$, then the ligand orbitals are separated into two orthogonal molecular orbitals as

$$p_\sigma \equiv \frac{1}{2}(q_{0\sigma} + q_{1\sigma} + Q_{0\sigma} + Q_{1\sigma}), \qquad (2.3)$$

and

$$P_\sigma \equiv \frac{1}{2}(q_{0\sigma} - q_{1\sigma} + Q_{0\sigma} - Q_{1\sigma}). \qquad (2.4)$$

Consequently, the single-M cluster is reduced to that in Fig. 2(c). Now we can regard the d-p unit as an effective subsystem of the $d(t_{2g})$-$L(t_{2g})$ one, and the D-P unit as an effective subsystem of the $d(e_g)$-$L(e_g)$ one, where L stands for ligand molecular orbital.[8]

To evaluate hopping energies, we apply the effective hybridization theory separately to e_g and t_{2g} orbitals. For t_{2g} (d) orbitals, the starting point is the equation[4]

$$\max\{\langle d^0|H|d^1\underline{p}\rangle\} = \max\{\langle d^0|H|d(t_{2g})^1\underline{L}(t_{2g})\rangle\},$$

where

$$|d^1\underline{p}\rangle = \frac{1}{\sqrt{2}}\sum_\sigma d^\dagger_\sigma p_\sigma|d^0\rangle.$$

As suggested by eq. (2.3), the left hand side is given by $\sqrt{2}\times 2v_1$, where $\sqrt{2}$ represents the contribution of spin degeneracy. The right hand side is given by $\sqrt{6}V(t_{2g})$, where $V(t_{2g})$ is the hybridization strength of a TiO_6 cluster model. Hence we have $v_1 = \sqrt{3}V(t_{2g})/2$. Similarly, v_2 is estimated as $v_2 = V(e_g)/\sqrt{2}$. For $V(e_g) = 3.0$ and $V(t_{2g}) = -1.5\,\text{eV}$,[3] we have $v_1 = u_1 = 1.3$ and $v_2 = u_2 = 2.1\,\text{eV}$. Other parameters are chosen to be the same as ref. 3: $\Delta = 4.0$, $10Dq = 1.7$, $U_{d1} = U_{d2} = 4.0$ and $U_{dc} = 6.0\,[\text{eV}]$.

Uozumi[9] and Taguchi[10] report approximately the same value of U_{dd}, U_{dc}, $10Dq$, and $V(e_g)$ as those of TiO_2 in their analyses on Ti $2p$-XPS of Ti_2O_3, so that we take the same parameter also for d^1 systems.[11]

In addition to the doubly-degenerate models, we define also nondegenerate models by removing the D and Q degrees of freedom from the degenerate model. The value of the parameter set including d-p hopping energy v, CT energy Δ, on-site d-d Coulomb energy U_{dd}, and on-site core-d attractive interaction U_{dc} will be explained in the subsequent section.

2.2 Spectral functions

In the present model, X-ray absorption and emission processes at a metal site l are described with the following operators:

$$T^{\mathrm{a}}(l) = \sum_{\sigma} (d^{\dagger}_{l\sigma} + D^{\dagger}_{l\sigma}) c_{l\sigma}, \tag{2.5}$$

$$T^{\mathrm{e}}(l) = \sum_{\sigma} c^{\dagger}_{l\sigma} (d_{l\sigma} + D_{l\sigma}). \tag{2.6}$$

The transition operator of RXES is now defined by

$$T(\Omega) \equiv \sum_{l} T^{\mathrm{e}}(l) G_0(\Omega) T^{\mathrm{a}}(l),$$

where $G_0(\Omega)$ is the resolvent operator defined as $G_0(\Omega) = (\Omega + E_g - H + \mathrm{i}\Gamma)^{-1}$. We use the value of $\Gamma = 0.4\,\mathrm{eV}$ throughout the present study, considering, first, the energy width of the intermediate state due to the Auger decay process,[12] second, the experimental resolution of the incident X-ray, and third, finite energy interval of eigenstates due to finite cluster size. It is worth noting that the point group symmetry of operators $d_{l\sigma} G_0 d^{\dagger}_{l\sigma}$ and $D_{l\sigma} G_0 D^{\dagger}_{l\sigma}$ is different from that of $d_{l\sigma} G_0 D^{\dagger}_{l\sigma}$ and $D_{l\sigma} G_0 d^{\dagger}_{l\sigma}$. The latter leads to final states with a different local point group symmetry from the ground state. As will be discussed, it brings about a class of nonbonding final states.

With the above operator, the spectral function of RXES is defined by

$$F_{\mathrm{RXES}}(\omega;\Omega) = \sum_{f \neq g} |\langle f|T(\Omega)|g\rangle|^2 \delta(E_f + \omega - E_g - \Omega).$$

We concentrate our attention to inelastic scattering in the present study. Similarly, the spectral function of XAS is written as

$$F_{\mathrm{XAS}}(\Omega) = \sum_{m} |\langle m(0)|T^{\mathrm{a}}(0)|g\rangle|^2 \delta(\Omega - E_m + E_g),$$

where $|m(0)\rangle$ is a final state with a core hole at $l = 0$. In addition, we define the spectral function of NXES as[4]

$$F_{\mathrm{NXES}}(\omega) = \int \mathrm{d}\varepsilon D(\varepsilon) \sum_{f,\sigma} |\langle f|T^{\mathrm{e}}(0) G_0(\Omega - \varepsilon) c_{0\sigma}|g\rangle|^2 \times \delta(\omega + E_f + \varepsilon - \Omega - E_g),$$

where $D(\varepsilon)$ is the density of states of the continuum level ε, and we will take it as a given constant. Because of the integration with respect to ε, F_{NXES} has no dependence on Ω in principle.

§3. Calculated Results I: Band Insulators

3.1 Nondegenerate d^0 system

To elucidate the role of orbital degeneracy, we first recapitulate results of nondegenerate models, where the parameter set $\Delta = 4.0$, $U_{dd} = 4.0$, $U_{dc} = 6.0$, and

$$v = \sqrt{(2v_1)^2 + (2v_2)^2}/2 = 3.5\,\mathrm{eV}$$

are used. These are the same as those in our previous paper.[4] For all XAS, RXES and NXES spectra in the present paper, the momentum-transfer q is fixed to be zero, and calculated line spectra are convoluted with Lorentzian 1.0 eV (HWHM). Moreover, the z-component of the total spin S_z is taken to be zero except for single-M cluster calculations with d^1 filling.

Figures 3(a) and 3(b) show the calculated spectra with nondegenerate single- and multi-M cluster models. Detailed discussions on the spectra have been given in the previous paper[4] with special attention to the appearance of the fluorescence-like spectra in the multi-M cluster model, as well as the fact that only the Raman component is observed in the single-M cluster calculation.

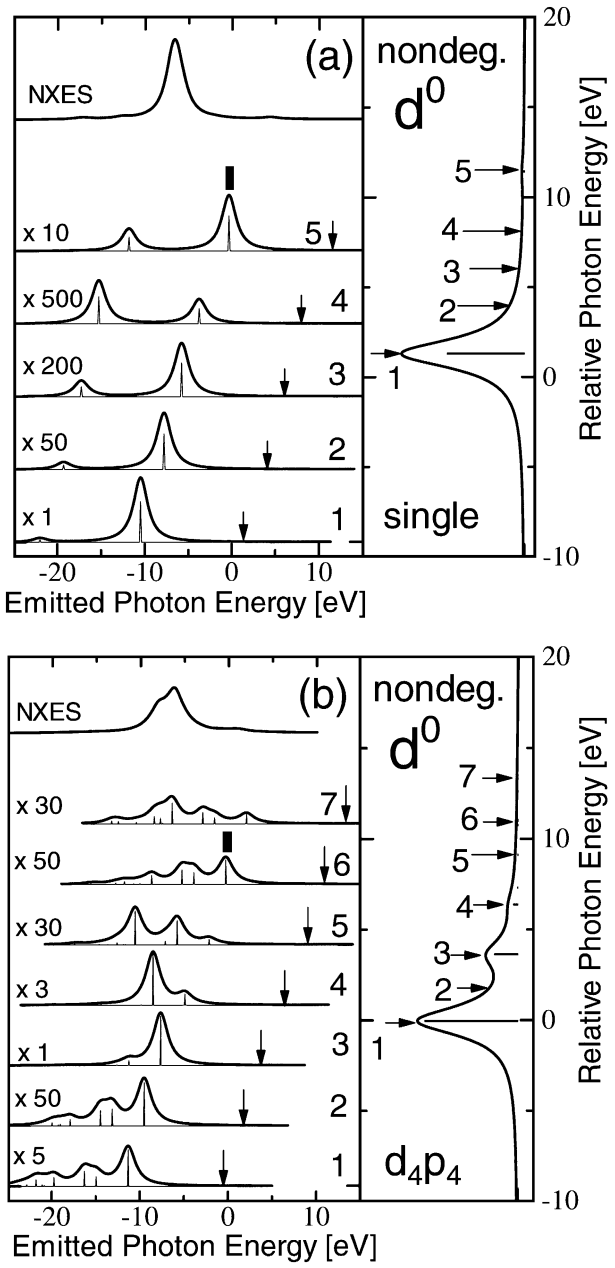

Fig. 3. XAS, RXES and NXES spectra calculated with *nondegenerate* models under d^0 filling, (a) the single-M and (b) d_4p_4 periodic clusters. For each figure, the right and left panels show XAS and RXES spectra, respectively. There is also a NXES spectrum at the top of the array of the RXES curves in the left panel. The arrows in each XAS spectrum indicate the position of excitation energies, and the numbers in the XAS spectra corresponds to those of RXES. The elastic scattering peaks are omitted from the figures, and they are replaced with the arrows. Each of original calculated RXES spectra is magnified by a rate indicated as "× 3".

Let us briefly review the bonding-antibonding separation in the XAS and RXES spectra within the single-M cluster model. When photoexcited, there are only two states $\{|\underline{c}d^1\rangle, |\underline{c}d^2\underline{L}\rangle\}$ in the Hilbert space of the single-

M cluster. Diagonalizing the 2×2 Hamiltonian matrix, we have the energy separation W_0' between the bonding and antibonding states as

$$W_0' = \sqrt{(\Delta + U_{dd} - U_{dc})^2 + 8v^2} \simeq 10.1\,\mathrm{eV}.$$

Similarly, in the final state of RXES, the bonding-antibonding separation is roughly estimated within so-called two-configuration approximation,

$$W_0 = \sqrt{\Delta^2 + 16v^2} \simeq 14.6\,\mathrm{eV}.$$

Note that matrix element $\langle d^1\underline{L}|H|d^0\rangle$ is $\sqrt{2}\times\sqrt{2}v$, where the first $\sqrt{2}$ originates from the spin degeneracy. These formulae will give a rough estimation on the bonding-antibonding separation also in degenerate models.

3.2 Degenerate d^0 system

Figure 4(a) shows XAS, NXES and RXES spectra calculated with the degenerate single-M cluster model. In the XAS spectrum, we observe two strong peaks and a number of subpeaks in their high-energy tail. Experimentally, four distinct peaks are observed in the main structure of Ti $2p$-$3d$ XAS of d^0 compounds such as TiO_2 and $FeTiO_3$.[1, 13] Since our model does not include the spin-orbit interaction of the core level, the two experimental peaks with lower energies correspond to the calculated main structure.

We also see that the RXES spectra depend on the incident photon energy Ω rather than the simple Raman component in the case of the nondegenerate single-M cluster. For lower Ω's such as 1 and 2, the single spectrum which linearly shifts as Ω increases is observed. This inelastic spectrum highlighted with blank bars survives for higher Ω's, whereas another spectrum highlighted with the shaded bar suddenly appears for 5 and 6. This type of enhancement when Ω is targeted at a satellite peak of XAS is also observed in the nondegenerate case, as marked also with shaded bars in Fig. 3(a). However, the nondegenerate results have no peaks corresponding to the series of peaks marked with blank bars in Fig. 4(a). Hence, we conclude that this series of peaks originates from the orbital degeneracy. By the reason discussed below, we call these peaks nonbonding ones hereafter.

To understand the origin of the inelastic spectra, consider the case of isotropic limit that $10Dq \to 0$ and $v_1 \to v_2$. In this case, the single-M Hamiltonian is ruled by two symmetries: the point group symmetry and the permutation symmetry between $\{d, p\}$ and $\{D, P\}$. Let us confine ourselves within the two-configuration approximation. The Hilbert space in the final state is decomposed by symmetry into two classes. One is composed of those states in which the above two symmetries are the same as those of the unperturbed ground state $|0_0\rangle \equiv |d^0\rangle$, and the other contains states with different symmetries from $|0_0\rangle$. Evidently, the former subspace is spanned by $|0_0\rangle$ and

$$|1_0\rangle = \frac{1}{2}\sum_\sigma (d_\sigma^\dagger p_\sigma + D_\sigma^\dagger P_\sigma)|d^0\rangle.$$

With a matrix element

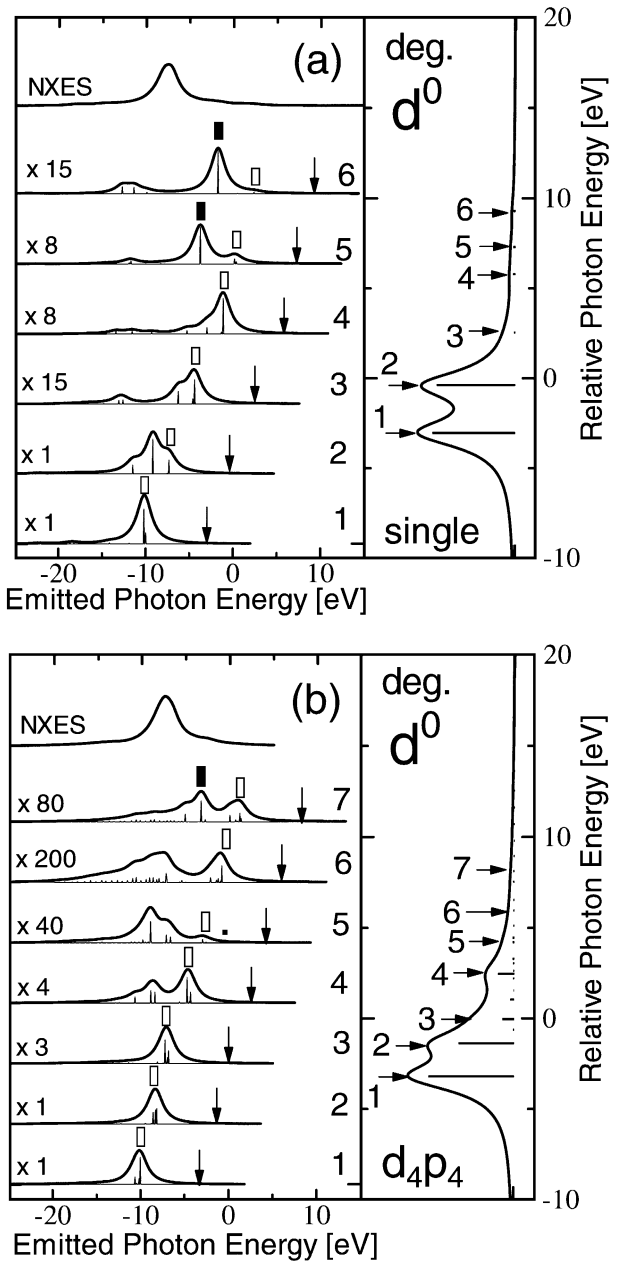

Fig. 4. XAS, RXES and NXES spectra calculated with *degenerate* models under d^0 filling, (a) the single-M and (b) d_4p_4 periodic clusters. See the caption for Fig. 3.

$$V_{\mathrm{eff}}(d^0) \equiv \langle 1_0|H|0_0\rangle = \sqrt{2[(2v_1)^2 + (2v_2)^2]},$$

the 2×2 eigenvalue problem shows that the energy separation between the bonding (ground) and antibonding states is just W_0, although calculated spectra exhibit somewhat smaller value than W_0.[14] Similarly to the nondegenerate case, $|g\rangle$ is the bonding state with relatively large $|0_0\rangle$ weight, and the antibonding state has relatively large $|1_0\rangle$ weight. Since the transition operators are symmetric as to the permutation, all allowed intermediate states have the same symmetry as $|g\rangle$ in this case. In the two-configuration approximation, each of them is a linear combination of

$$|1_0'\rangle = \frac{1}{2}\sum_\sigma (d_\sigma^\dagger + D_\sigma^\dagger)c_\sigma|0_0\rangle,$$

and

$$|2'_0\rangle \propto \sum_\sigma (d^\dagger_\sigma + D^\dagger_\sigma)c_\sigma|1_0\rangle,$$

giving bonding and antibonding intermediate states. Since $\Delta + U_{dd} - U_{dc} > 0$, the bonding intermediate state has mainly $|1'_0\rangle$ weight, and would have large overlap with $(d^\dagger_\sigma + D^\dagger_\sigma)c_\sigma|g\rangle$. Similarly, the antibonding intermediate state has large overlap with $(d^\dagger_\sigma + D^\dagger_\sigma)c_\sigma|\mathrm{AB}\rangle$, where $|\mathrm{AB}\rangle$ is the antibonding final state. Consequently, absorption intensity strongly concentrates at the main peak, and $|\mathrm{AB}\rangle$ is strongly enhanced when Ω is tuned at the satellite peak in the XAS spectra.

The latter subspace containing different symmetries from that of $|g\rangle$ gives rise to the nonbonding states. In the isotropic limit under the two-configuration approximation,

$$|\mathrm{N}1_0\rangle \equiv \frac{1}{2}\sum_\sigma (d^\dagger_\sigma P_\sigma + D^\dagger_\sigma p_\sigma)|d^0\rangle$$

contributes to inelastic scattering. This state has the same permutation symmetry as that of the ground state, but the local point group symmetry is different. By the reason explained above, it is the elastic line (ground state) that is the most strongly enhanced when Ω is tuned at the main absorption manifold. The elastic line is, however, omitted from the figures, so that the main inelastic spectra originate from the nonbonding states for that Ω. By definition, the existence of the nonbonding states is a direct consequence of orbital degeneracy. The nonbonding state is energetically Δ higher than $|d^0\rangle$, being nearly independent of hybridization strength. Since the energy of the bonding state is estimated as $(\Delta - W_0)/2$ within the two-configuration approximation, the nonbonding state will be observed

$$W_{0\mathrm{N}} \equiv (\Delta + W_0)/2$$

distant from the elastic line. Note that this is always smaller than W_0, and therefore the nonbonding state is located in between the bonding and antibonding states in any case.

When a finite $10Dq$ is introduced, we have a finite energy difference between $\underline{c}d^1$- and $\underline{c}D^1$-dominant intermediate states due to $10Dq$, so that we observe the doubly-peaked structure in the main manifold of the XAS spectrum. Similarly, the nonbonding lines split into several ones in a RXES spectrum. Since the Hamiltonian is now not symmetric as to the permutation, an antisymmetric state

$$|\mathrm{N}2_0\rangle \equiv \frac{1}{2}\sum_\sigma (d^\dagger_\sigma p_\sigma - D^\dagger_\sigma P_\sigma)|d^0\rangle$$

appears as a nonbonding peak in the final state. This state has the same local point group symmetry as the ground state. Furthermore, $|\mathrm{N}1_0\rangle$ split into the following two states:

$$|\mathrm{N}1_0 1\rangle \equiv \frac{1}{\sqrt{2}}\sum_\sigma d^\dagger_\sigma P_\sigma|d^0\rangle$$

$$|\mathrm{N}1_0 2\rangle \equiv \frac{1}{\sqrt{2}}\sum_\sigma D^\dagger_\sigma p_\sigma|d^0\rangle,$$

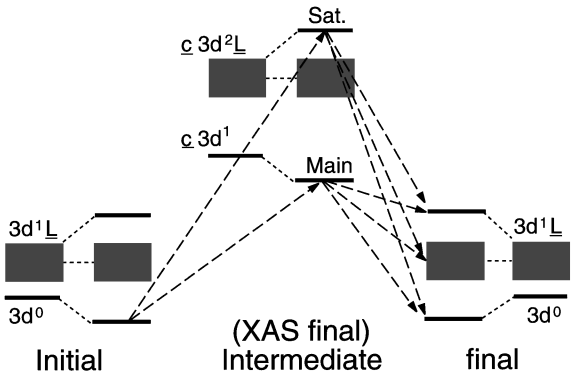

Fig. 5. The energy scheme of M 3d-2p RXES of d^0 compounds in the standard notation. In the initial and final states, the metal-ligand hybridization creates the bonding (represented with the lowest horizontal bar), antibonding (the highest bar) and nonbonding states (the shaded rectangle). These three kinds of states similarly exist in the intermediate state. While the d-p hybridization gives rise to the bonding-antibonding separation, the energy of nonbonding states is hardly perturbed with the hybridization.

with energy separation of order of $10Dq$. Thus, we observe three nonbonding lines in this case. Generally, anisotropy of v_1 and v_2 gives rise to energy shift of the nonbonding peaks. As a result, $\mathrm{N}1_0 1$- and $\mathrm{N}2_0$-dominat states are accidentally seen at nearly the same position in Fig. 4(a). The transition processes in the single-M cluster is summarized in Fig. 5, where these three nonbonding states are represented with the shaded rectangle. Note that the nonbonding states are hardly perturbed with the metal-ligand hybridization.

These features of the degenerate single-M cluster calculation are substantially conserved in the multi-M cluster calculation. Apart from subpeaks such as 4, the main manifold of the XAS spectrum shown in Fig. 4(b) is composed of two definite lines, and we can naturally attribute these lines to those states which have relatively large $\underline{c}d^1$ or $\underline{c}D^1$ weight in the photoexcited cluster. For RXES spectra, we see, firstly, that the nonbonding states give the main inelastic structure for the main peak resonance (spectrum 1 and 2). Secondly, the antibonding state marked with the shaded bar is strongly enhanced when Ω is tuned in the vicinity of the satellite peak (spectrum 7), although the satellite peak is greatly smeared out and does not give a clear structure.

Close inspection shows, however, certain modifications are observed in the spectra of local origin. Firstly, while the nonbonding states keep energy separation of order of $10Dq$ in the single-M cluster calculation, the separation in Fig. 4(b) is considerably contracted because of the finite transfer between unit clusters. Whether or not this is the case in realistic three-dimensional systems is unclear because whether the separation between the nonbonding states get smaller or larger would greatly depend on a band structure. Secondly, the intensity ratio of the main XAS peaks is slightly changed. This is possibly associated with a change in character of the main absorption peaks, from the simple bonding state to a core-excitonic state.

The most conspicuous change in RXES spectra is oc-

currence of the fluorescence-like spectra. Figure 4(b) exhibits those inelastic spectra whose position is almost the same as that of NXES for almost all Ω's higher than 3. This is sharp contrast to the nonbonding-antibonding spectra explained above, which behave as if NXES spectrum has no relation with RXES. Similarly to the nondegenerate case, we confirm again that the origin of such spectra is itinerancy in the targeted intermediate state. The subpeaks in the high-energy tail of the main absorption peaks, such as 3, 4 and 5 in Fig. 4(b), originate from a finite number of k-points, and highly itinerant according to the core exciton theory. In fact, a detailed analysis of the present authors shows that a photoexcited electron in the intermediate state 3 is delocalized mainly through the d-p transfer path, and that a photoexcited electron in the intermediate states 4 and 5 is delocalized mainly through the D-P transfer path.

§4. Calculated Results II: Mott-Hubbard Insulators

4.1 Nondegenerate d^1 system

Figure 6 shows calculated XAS, NXES and RXES spectra with nondegenerate models with d^1 filling, which simulates the t_{2g} bands of Ti_2O_3. The parameters are taken as $v = 2.0$, $\Delta = 2.0$, $U_{dd} = 4.0$ and $U_{dc} = 6.0\,\mathrm{eV}$.[9] Because of $U_{dd} + \Delta > U_{dd}$, this system is in the MH regime in the Zaanen-Sawatzky-Allen diagram.[15] Note that the lowest charge excitation is made by an inter-site d-d excitation in this case. Then it is interesting to study RXES spectra of MH systems in the context of the nonlocal (or large-cluster) effects.

In the nondegenerate single-M cluster model with d^1 filling, the only possible configuration in the intermediate state is $\underline{c}d^2$, so that we have the only single peak in XAS spectra in Fig. 6(a). On the other hand, two configurations of d^1 and $d^2\underline{L}$ are possible in the final state. Thus, we observe the only inelastic peak due to charge-transfer

$$W_1 = \sqrt{(\Delta + U_{dd})^2 + 8v^2} \simeq 8.2\,\mathrm{eV},$$

distant from the elastic line, and the RXES spectra exhibit necessarily only Raman component.

In the NXES spectrum in Fig. 6, we see a strong peak at about $-2\,\mathrm{eV}$ and a weak structure at about $-10\,\mathrm{eV}$. The former corresponds to a d^0-dominant state, and the latter to a $d^1\underline{L}$-dominant state.

In addition to the CT peak, the inter-site d-d excitation should take part in RXES spectra in the multi-M cluster model. There is observed an inelastic peak approximately 4.4 eV distant from the elastic line in RXES spectra in Fig. 6(b). While spectral weight of this peak is strong for lower Ω's up to 5, a structure about 10 eV distant from the elastic line is enhanced for Ω's higher than 5. To study these structures, we calculate valence photoemission spectra (PES) and bremsstrahlung isochromat spectra (BIS), whose spectral functions are written as

$$F_{\mathrm{PES}}(k,\omega) = \sum_f |\langle f|d_{k,\uparrow}|g\rangle|^2 \delta(\omega + E_f - E_g), \quad (4.1)$$

$$F_{\mathrm{BIS}}(k,\omega) = \sum_f |\langle f|d^\dagger_{k,\uparrow}|g\rangle|^2 \delta(\omega - E_f + E_g). \quad (4.2)$$

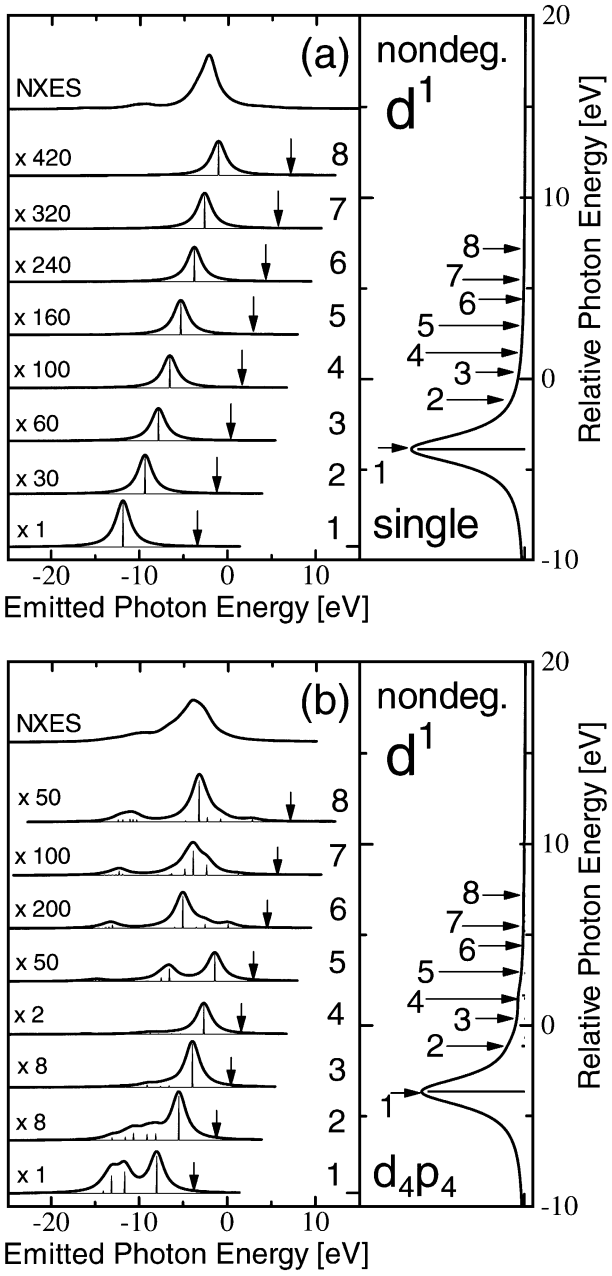

Fig. 6. XAS, RXES and NXES spectra calculated with *nondegenerate* models under d^1 filling, (a) the single-M and (b) d_4p_4 periodic clusters. See the caption for Fig. 3.

Figure 7 shows PES and BIS spectra, where we adopt a nondegenerate d_8p_8 cluster model with the same parameters to take more k-points. The figure clearly shows that the upper branch of the simple Bloch bands in the $U_{dd} \to 0$ limit (solid curves)

$$\varepsilon^{\pm}(k) - \varepsilon_0 = \frac{\Delta}{2}\left(1 \pm \sqrt{1 + (4v/\Delta)^2 \cos^2(k/2)}\right),$$

is substantially modified into the lower Hubbard band (LHB) and upper Hubbard band (UHB). Hence we attribute the aforementioned lower energy structure in RXES to a CT process, and the higher energy one to an inter-site d-d transfer, which rules the Mott-Hubbard gap. We call the former one "CT" and the latter "MH" hereafter. Furthermore, the intense peak at $-4\,\mathrm{eV}$ in the NXES spectrum (Fig. 6(b)) is attributed to a radia-

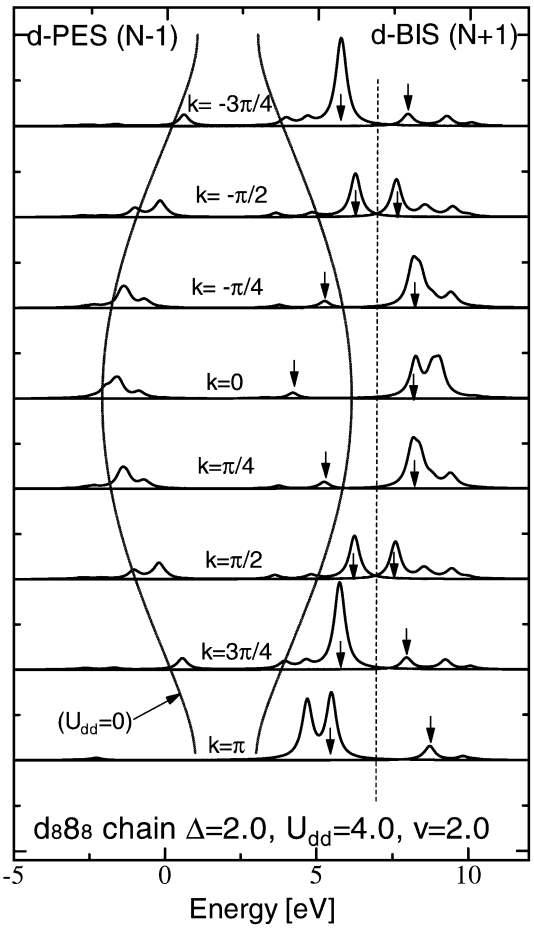

Fig. 7. PES and BIS spectra calculated with the d_8p_8 *non-degenerate* chain. The calculated spikes are convoluted with Lorentzian 0.2 eV (HWHM). The solid curves show the Bloch bands in the $U_{dd} \to 0$ limit. The arrows show the upper and lower Hubbard bands. The Fermi level is represented with the dotted line. We take ε_0 as the origin of the energy.

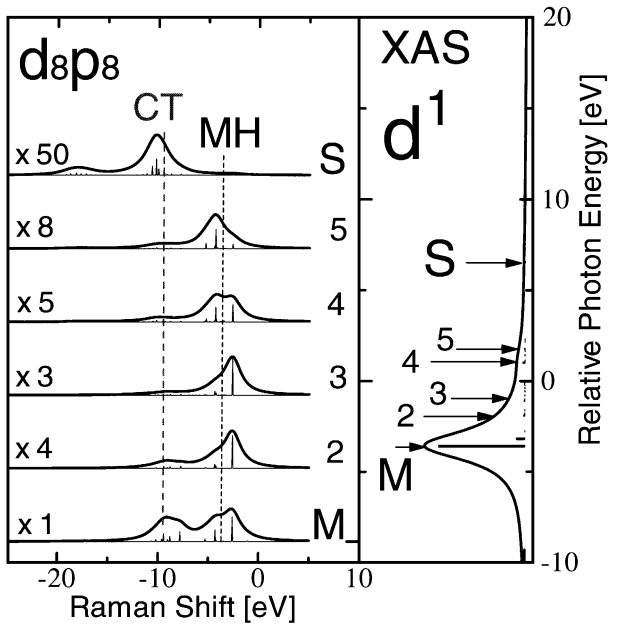

Fig. 8. RXES and XAS spectra calculated with the d_8p_8 *nondegenerate* chain. Note that the abscissa is defined as Raman shift $\omega - \Omega$, which is the same as $E_g - E_f$. The elastic line, which should reside at zero, is omitted from the figure. The excitation energies and the numbers attached to the arrows in the XAS spectrum corresponds to those in the RXES spectra.

tive transition from LHB, whereas a bump in its low energy tail to a radiative transition from the lowest valence band. The difference in intensity is naturally explained by difference in d-weight of these bands.

Although the MH structure in Fig. 6(b) is composed of the single line, there should be generally energy dispersion in this structure. To confirm this, we show XAS and RXES spectra calculated with the d_8p_8 cluster in Fig. 8, where all RXES spectra are plotted as a function of Raman shift. The MH structure is clearly seen at about -3.5 eV, and the CT structure at about -9.5 eV. We observe energy dispersion of the MH structure for spectra 4 and 5. Corresponding to the fact that only $|\underline{c}d^2\rangle$ is possible in the single-M cluster limit, the XAS spectrum has the strong peak labeled with M, as in Fig. 6(b). The additional peaks are also observed in its high-energy tail. Their characters are depicted schematically in Fig. 9(a), where each transition process between many-body states is mapped into a counterpart in the one-electron picture. In the states corresponding to the main peak M and the very weak satellite peak S, the core hole is mainly screened by the photoexcited electron itself. The peaks 4 and 5 correspond to the excitation to UHB. These are necessarily delocalized and poorly-screened. The peaks 2 and 3 have an intermediate character of the two states, and they are irrelevant to be depicted as a one-electron process.

Similarly, RXES final states are visualized in Fig. 9(b) in terms of the one-electron density of states. The MH structure is related to one electron-hole pair creation between UHB and LHB, whereas the CT one between UHB and the filled ligand band. The dispersive Ω-dependence for the spectra 4 and 5 is directly associated with energy dispersion of UHB. Although this behavior is somewhat similar to the fluorescence-like spectra, its energy width is too narrow under the realistic parameter set for Ti oxides[16] to explain the experimental trend of, *e.g.*, Ti_2O_3.[7]

4.2 Degenerate d^1 system

Figure 10 shows XAS, NXES and RXES spectra calculated with degenerate single-M cluster and d_4p_4 models with d^1 filling. We fixed $S_z = 1/2$ for the single-M cluster calculation.

Let us first consider the single-M cluster case. We see that the main manifold of the XAS spectrum exhibits a doubly-peaked structure. This is consistent to the d^0 calculation, but the lower energy absorption peak is considerably suppressed because of larger occupation number in the lower energy d-orbital. We also see that the higher branch of the main manifold in Fig. 10(a) is composed of a few peaks with extremely small energy separation. This is attributed to the contribution of spin multiplet. When Ω is tuned at these peaks, the resultant final state would have large D^1 weight. Thus a strong inelastic peak observed 2.5 eV distant from the elastic peak

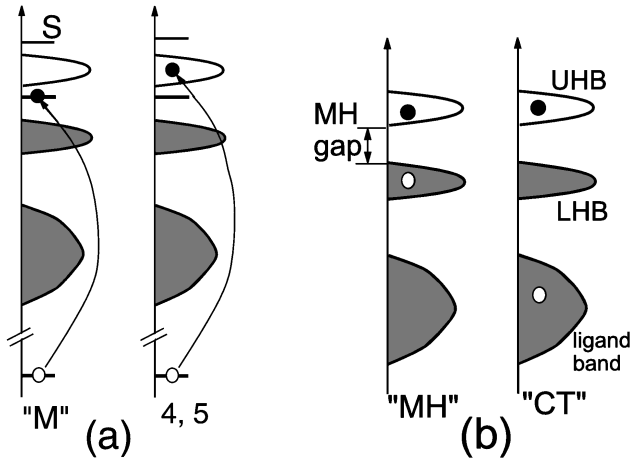

Fig. 9. Schematic explanation of representative final states in XAS and RXES spectra. The shaded and blank areas show occupied and unoccupied densities of states, respectively. The closed and open circles represent an electron and hole, respectively. (a) In the intermediate (XAS final) state, a core electron is photoexcited to bound states (represented with bars) or UHB. The labels M, S, 4 and 5 correspond to those in Fig. 8. (b) An electron-hole pair is left in the final state.

in RXES spectrum 2 is attributed to the intra-site d-d excitation from the d to the D orbital. We denote this excitation by "d-d" hereafter. Note that the value 2.5 eV is the same order of $10Dq$, but from a quantitative point of view, it considerably deviates from $10Dq$ because of relatively large anisotropy of v_1 and v_2.

In addition to the d-d peak, another structure is observed about 10 eV distant from the elastic line. This is attributed to charge-transfer to the metal site from the neighboring ligand sites. To study the origin of inelastic peaks clearly, we arrange the same RXES spectra with Raman shift in Fig. 11(a), where one sees that the CT structure is distributed over about 4 eV. Unlike the d^0 case, the permutation symmetry does not rule the separation between antibonding and nonbonding states when a finite $10Dq$ works, because the unperturbed state $|1_1\rangle \equiv d^\dagger_\uparrow|d^0\rangle$ is not symmetric. Within the two-configuration approximation, there are two other state vectors, which have the same point group symmetry as $|1_1\rangle$,

$$|2_1 1\rangle \equiv d^\dagger_\downarrow p_\downarrow |1_1\rangle$$
$$|2_1 2\rangle \equiv \frac{1}{\sqrt{2}} \sum_\sigma D^\dagger_\sigma P_\sigma |1_1\rangle.$$

Both of them have a doubly-occupied metal site. Consider a linear combination of these vectors, $|2_1\rangle$, under condition such that $|\langle 2_1|H|1_1\rangle|$ is maximized. Following the effective hybridization theory,[4] we have

$$|2_1\rangle = \frac{2}{V_{\rm eff}(d^1)} \left(v_1|2_1 1\rangle + \sqrt{2}v_2|2_1 2\rangle \right),$$

where

$$V_{\rm eff}(d^1) \equiv \sqrt{(2v_1)^2 + 2(2v_2)^2}.$$

Diagonalizing the 2×2 Hamiltonian spanned by $\{|1_1\rangle, |2_1\rangle\}$, we have bonding-antibonding separation

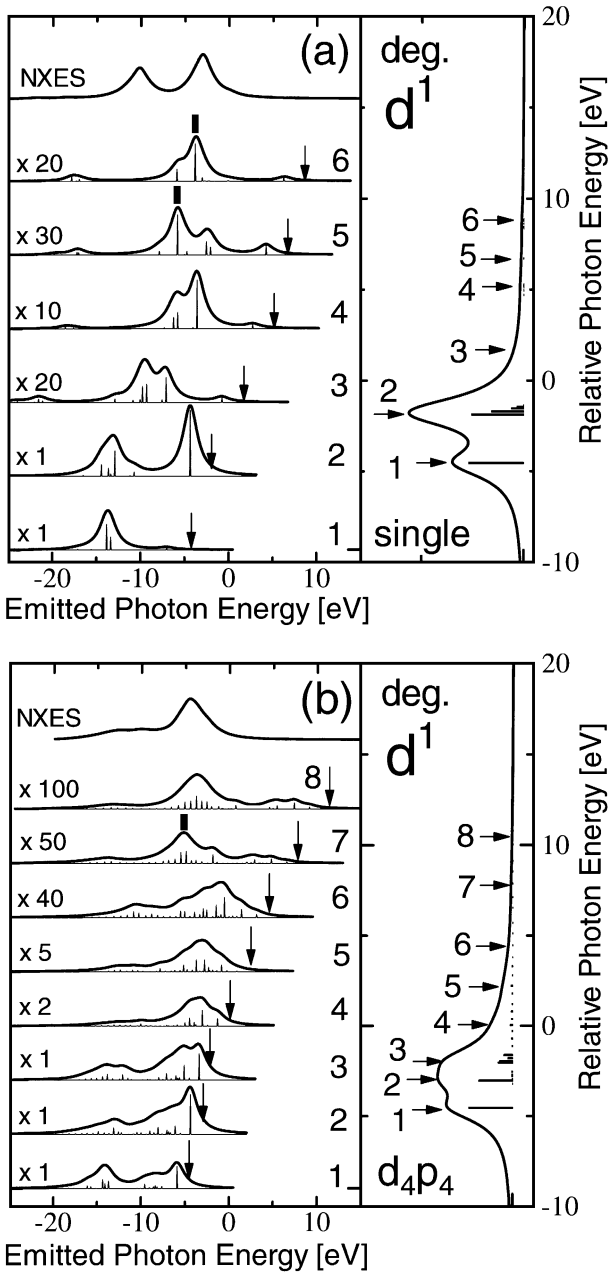

Fig. 10. XAS, RXES and NXES spectra calculated with the *degenerate* models under d^1 filling, (a) the single-M and (b) d_4p_4 periodic clusters. See the caption for Fig. 3.

$$W_1 \simeq \sqrt{(\Delta + U_{dd})^2 + 4V^2_{\rm eff}},$$

which is the same order of W_0. A peak at -12.6 eV labeled with "AB" in Fig. 11(a) originates from this antibonding state, and it is strongly enhanced when Ω is tuned at the satellite structures 5 and 6, being consistent to the d^0 case. This is also described in Fig. 10(a) with the shaded bars.

In this context, we consider the state orthogonal to $|2_1\rangle$ as the nonbonding state in the truncated Hilbert space,

$$|{\rm N}2_1\rangle = \frac{2}{V_{\rm eff}(d^1)} \left(-\sqrt{2}v_2|2_1 1\rangle + v_1|2_1 2\rangle \right).$$

This corresponds to a peak at -8.8 eV, which is strongly

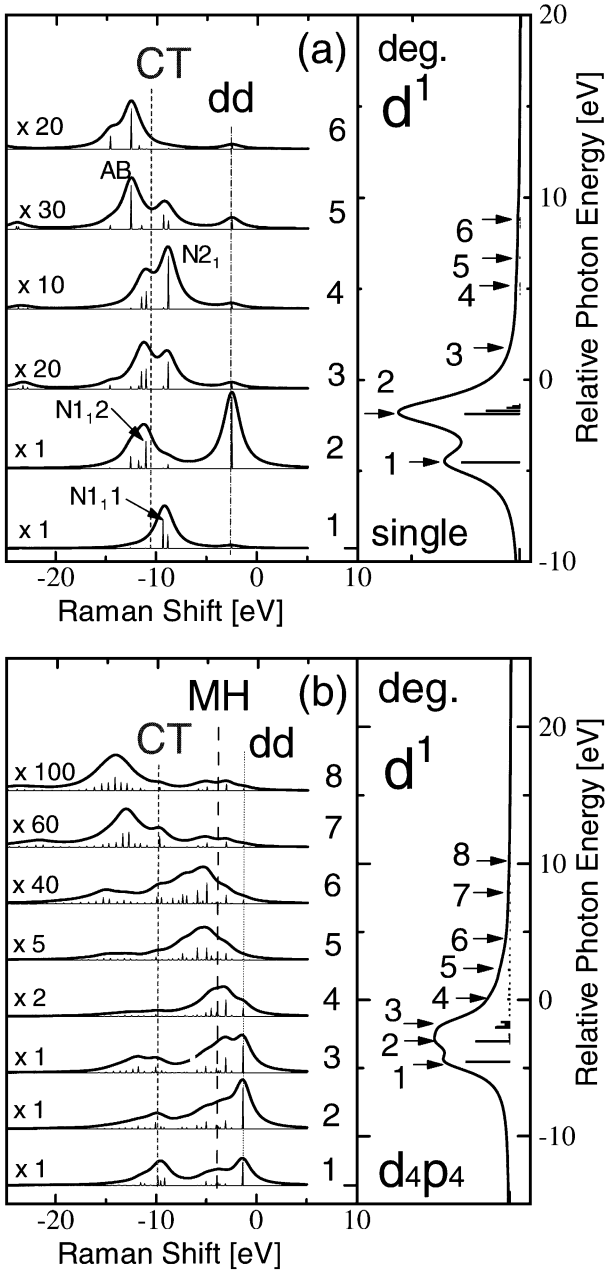

Fig. 11. RXES and XAS spectra for d^1 filling calculated with (a) the degenerate single-M and (b) degenerate d_4p_4 cluster models. All excitation energies and the numbers attached to the arrows are the same as in Fig. 10. See the caption for Fig. 3.

enhanced in the RXES spectrum 4. This fact suggests that the absorption spectra in the vicinity of the arrow labeled with 4 have also nonbonding character. In fact, it has relatively large weight in $|\underline{c}D^1; d^2\underline{p}\rangle$, which gives rise to relatively large $|2_1 1\rangle$ weight after radiative transition of the D electron.

There is another class of nonbonding states, which has different point group symmetry from $|g\rangle$. When Ω is tuned at the main absorption peaks, it is this class of states that are the most strongly enhanced, as in the d^0 case. Corresponding to $|\mathrm{N}1_0 1\rangle$ and $|\mathrm{N}1_0 2\rangle$, state vectors such as

$$|\mathrm{N}1_1 1\rangle \equiv d^\dagger_\downarrow P_\downarrow |1_1\rangle$$

$$|\mathrm{N}1_1 2\rangle \equiv \frac{1}{\sqrt{2}} \sum_\sigma D^\dagger_\sigma p_\sigma |1_1\rangle$$

are of this kind. The former contributes to an inelastic peak at -9.3 eV when Ω is tuned at the peak 1, whereas the latter contributes an inelastic peak at -11.3 eV when Ω is tuned at the peak 2. The energy separation between them is naturally attributed to $10Dq$.

Apart from the d-d structure, the Ω dependence of RXES spectra has much in common with the d^0 spectra in Fig. 4(a) rather than the nondegenerate calculation in Fig. 6(a). The multi-M cluster (d_4p_4) results are shown in Figs. 10(b) and 11(b). In contrast to the single-M cluster results, we observe fluorescence-like behavior there. Note that the nondegenerate multi-M cluster calculation in Fig. 6(b) exhibits no such behavior. Thus we conclude that it is essential for the appearance of the fluorescence-like spectra in d^1 systems to include orbital degeneracy.

The other large-cluster effect is inelastic peaks due to inter-site d-d excitations. Compare Fig. 11(b) with Fig. 8. As explained, the latter model is regarded as a truncated model to include only the d-p transfer path of the former. We notice that a bump at about -4 eV in Fig. 11(b) for RXES spectra 1, 2, 3 and 4. This is attributed to the inter-site d-d excitation, and labeled with "MH", as in Fig. 8. Although the MH structure is separated from the CT structure in Fig. 8, one observes that the center of the spectral weight moves to lower energy roughly proportional to Ω, from MH to CT structure and beyond, resulting in the fluorescence-like spectra in Fig. 11(b).

On the other hand, we see that a structure at about -10 eV is enhanced for 1 and 2, and a structure at about -11.9 eV is enhanced for 3. This is explained by the enhancement of the nonbonding states which originate from $|\mathrm{N}1_1 1\rangle$, $|\mathrm{N}1_1 2\rangle$ and $|\mathrm{N}2_1\rangle$. We also observe an isolated peak at -1.4 due to the intra-site d-d excitation. The resonance enhancement of the antibonding peak is also observed for the spectrum 7, as expressed with the shaded bar in Fig. 10(b). Figure 11(b) is very intriguing in that these structures of local origin, which are successfully explained with single-M cluster model, coexist with the aforementioned structures due to inter-site effects.

§5. Discussion

5.1 d^0 system

We defined a nonbonding state as that state which has no or little hybridization matrix element with the ground state. Mathematically, this definition may hold in realistic three-dimensional systems. Figures 4(a) and 4(b) show slight Ω-dependence in the nonbonding structure, where the spectral weight moves from higher energy to lower energy branch of the nonbonding peaks in going from the spectrum 1 to 3. As discussed within the single-M cluster model, the energy separation between the two nonbonding states, which originate from $|\mathrm{N}1_0 1\rangle$ and $|\mathrm{N}1_0 2\rangle$, is attributed mainly to $10Dq$. While this type of Ω-dependence is consistent to experimental fea-

ture,[5] the calculated spectra show considerable cluster size dependence of the separation. This is an example that a feature of local origin is renormalized by multi-M cluster effects. Apart from this type of slight dependence, the fact that Ω-dependence of the nonbonding structure is not very strong in experimental Ti $3d$-$2p$ RXES of TiO_2[5] suggests that the nonbonding structure is composed of states with various symmetries, and these states are highly smeared out by O $2p$ band effects.

The latest experimental data on Ti $3d$-$2p$ RXES of TiO_2[5] shows a strong resonance enhancement of a peak 14 eV distant from the elastic line, when Ω is tuned at the satellite structure of the XAS spectrum under a polarized configuration. This enhancement is not observed in refs. 1 and 13, where the *depolarized* configuration is adopted. This fact means that the CT excited state corresponding to the 14 eV peak is the same symmetry as $|g\rangle$, and we naturally attribute it to the antibonding state, whose origin is the higher energy eigenstate in the truncated Hilbert space spanned by $|0_0\rangle$ and $|1_0\rangle$. Despite of its simplicity, our model well explains the essential physics of the experimental 14 eV enhancement. Note that any model without U_{dc}[17] and also spinless exciton models[18] can not describe the CT satellite of XAS, and therefore by no means describe the experimental polarization dependence.

There had been a controversy on the origin of the satellite structure of Ti $2p$-XPS or $2p$-XAS of TiO_2.[3,19] Okada and Kotani conclusively demonstrated that it is the CT satellite by their theoretical analysis with a TiO_6 cluster model.[3] With this regard, the polarization dependence of RXES when Ω is tuned at the satellite structure is significant in that it dramatically proves its character as the CT satellite. Moreover, the large bonding-antibonding separation offers evidence that TiO_2 is in the strong hybridization regime. Thus, parameter estimations based on the atomic picture would be subtle in many cases.

Apart from the fluorescence-like behavior, the single-M cluster model well explained the Ω-dependence of RXES spectra calculated with the multi-M cluster model. This means that the local transition picture as shown in Fig. 5 is at least partly applicable to the Raman component despite the translational symmetry of the system. This is a consequence of the special feature of RXES that reflects local as well as itinerant nature of the system.

We comment on the relative intensity of the structures of local origin, i.e. the antibonding and nonbonding structures. Comparing Fig. 3 with Fig. 4, we see that they are clearer in the latter than in the former. This suggests a trend that the more available internal degrees of freedom a unit cluster has, the more weight of spectra of local origin is observed. The reason is naturally related to the number of transition paths.

5.2 d^1 system

We demonstrated the appearance of the intra-site d-d excitation in RXES spectra for d^1 systems. Recently Higuchi *et al.* reported that intensity of a peak 2.3 eV distant from the elastic line increases with La doping for $SrTiO_3$.[20] Since $La_xSr_{1-x}TiO_3$ has nominally d^x filling, their explanation that the 2.3 eV peak is caused by the intra-site $t_{2g} \rightarrow e_g$ transition seems to be natural. While they made estimation of the value of $10Dq$ simply as 2.3 eV, Fig. 11 shows considerable cluster size dependence of its energy separation from the elastic line. We have the value of 2.5 eV with the single-M cluster model, whereas 1.4 eV with the multi-M cluster model. Although the latter is fairly close to the actual value $10Dq = 1.7$ eV, whether or not this is the case in realistic three-dimensional systems is unclear because whether it gets smaller or larger would greatly depend on a band structure. What we can say definitely is that the anisotropy between t_{2g} and e_g orbitals play a certain role.

For the CT structure, Fig. 10 shows Ω-dependence similar to the results of the d^0 systems in Fig. 4. This is related to the fact that we can successfully define the antibonding state as explained in the preceding section. The lower symmetry of the unperturbed d^1 state, however, disturbs the resonance enhancement of the antibonding peak as compared to d^0. Analogous to TiO_2, there is a broad satellite structure in experimental Ti $2p$-XAS of Ti_2O_3.[7] Our results on d^1 systems predict that polarization dependence of the antibonding peak should be observed when Ω is tuned at the satellite structure.

For band insulators, we have confirmed that spatially extended states are in the high energy tail of the main manifold of XAS, and that these states maintain the one-electron character to great extent against the strong U_{dd} and U_{dc}. While we have some extended states also for MH insulators, they are quite unlike the simple one-electron states, but complicated many-electron states involving excitations in the Hubbard bands. It is not necessarily clear what kinds of extended states are created when orbital degeneracies are introduced in. What one can definitely say is that the orbital degrees of freedom relaxes the reduction effect due to the Pauli principle, and therefore encourages the dissipation of a photoexcited electron. In any case, the existence of highly delocalized states that are densely distributed over finite width in an absorption threshold is a necessary condition to display the fluorescence-like component in RXES spectra. Although Minami and Nasu[18,22] stressed the role of phonon degrees of freedom in the appearance of a fluorescence (or luminescence) component, our theory can explain essential features of experimental results in d^0 and d^1 systems without the electron-phonon coupling. We consider that the electron-phonon coupling plays a minor role in M $3d$-$2p$ RXES of $3d$ systems.

§6. Conclusions

We have discussed the role of orbital degeneracy in M $3d$-$2p$ RXES with periodic multi-M cluster models under d^0 and d^1 fillings. We first investigated d^0 systems with a single-M cluster model. Calculated RXES spectra showed only Raman component, which is composed of antibonding and nonbonding states. The origin of the antibonding state comes from totally symmetric states as to the permutation of degenerate orbitals, whereas that of the nonbonding state comes from those states which have different symmetry from the unperturbed ground

state $|d^0\rangle$. This mathematical definition well explains the Ω-dependence of RXES spectra, which is quantitatively consistent to the experimentally observed resonance enhancement of the antibonding state under a polarized configuration.

With a degenerate multi-M cluster model, we demonstrated that the above properties of local origin are substantially conserved in RXES spectra. Large-cluster effects, however, were observed, first, in the modulation of intensity ratio between two main absorption peaks, and second, in the reduction of the peak separation in the nonbonding structure. Moreover, third, we confirmed the appearance of the fluorescence-like RXES spectra, which is completely missing in the single-M cluster results.

Next we showed calculated results for d^1 systems. RXES spectra calculated with nondegenerate models exhibit only Raman component for both single- and even multi-M cluster models, but the latter results show considerable Ω-dependence. While a structure due to intersite d-d transition is enhanced for lower Ω, a structure due to CT is enhanced for higher Ω. Although energy dispersion of UHB slightly reflects on the Ω-dependence, it is too small to explain the occurrence of fluorescence-like spectra in realistic parameter set for Ti oxides.

The most remarkable effect of orbital degeneracy is the appearance of the fluorescence-like spectra in the multi-M cluster calculation, being qualitatively consistent to experimental spectra. The naive conjecture that effective hopping energy reduced by d-d on-site Coulomb interaction hinders the appearance of the fluorescence-like behavior does not hold when the orbital degeneracy is introduced. This result demonstrates the essential importance of the orbital degeneracy as well as the translational symmetry. The appearance of the fluorescence-like spectra seems to be *a general phenomenon that is observed wherever highly delocalized continuum states exist.*

In addition to the fluorescence-like spectra, the orbital degeneracy gives rise to, first, a peak due to the intra-site d-d excitation. The separation between this peak and the elastic line is of order of $10Dq$, but it considerably depends on cluster size. Second, nonbonding states as well as the antibonding state contribute to inelastic spectra. Despite the difference in symmetry of the ground state, the calculated results show the Ω-dependence similar to the d^0 case, from which resonance enhancement of the antibonding peak is predicted when Ω is tuned at the XAS satellite structure under polarized configurations.

Acknowledgements

The authors thank Y. Harada, Y. Tezuka and S. Shin for sending their experimental data and fruitful discussions. The authors also thank M. Matsubara for valuable discussion on numerical results with the impurity Anderson model. This work is partly supported by a Grant-in-Aid for Scientific Research from the Ministry of Education, Science and Culture. The computation in this work was done using the facilities of the Super-Computer Center, Institute for Solid State Physics, The University of Tokyo.

1) Y. Tezuka, S. Shin, A. Agui, M. Fujisawa and T. Ishii: J. Phys. Soc. Jpn. **65** (1996) 312.
2) C. F. Hague, M. Tronc, F. M. F. de Groot, H. Ogasawara, A. Kotani, J. H. Guo and C. Såthe: *Advanced Light Source Compendium of User Abstracts and Technical Reports, 1997.*
3) K. Okada and A. Kotani: J. Electron Spectrosc. Relat. Phenom. **62** (1993) 131.
4) T. Idé and A. Kotani: J. Phys. Soc. Jpn. **67** (1998) 3621.
5) Y. Harada, M. Matsubara, A. Kotani, T. Kinugasa, R. Eguchi and S. Shin: to appear in Phys. Rev. B **61** (2000) No. 19.
6) M. Matsubara, T. Uozumi, A. Kotani, Y. Harada and S. Shin: to appear in J. Phys. Soc. Jpn. **69** (2000) No. 5.
7) Y. Tezuka *et al.*, private communication.
8) The other choice that $v_1 = u_1$ and $v_2 = -u_2$ also leads to the exactly same single-M cluster as in Fig. 2(c). Since these two choices prove to be exactly equivalent even in the double-M cluster (periodic d_2p_2) case, it is conceivable that the conclusions in the present paper do not drastically depend on the choice at all.
9) T. Uozumi, K. Okada, A. Kotani, Y. Tezuka and S. Shin: J. Phys. Soc. Jpn. **65** (1996) 1150.
10) M. Taguchi: Thesis, Faculty of Science, Department of Physics, The University of Tokyo, 1998 [in Japanese].
11) Reference 10 reports a large CT energy of 6.5 eV. Note that this corresponds to $U_{dd} + \Delta - \frac{3}{5}10Dq$ in the notation of the present model, giving $\Delta = 3.52$ for $U_{dd} = 4.0$ and $10Dq = 1.7$.
12) M. O. Krause and J. H. Oliver: J. Phys. Chem. Ref. Data, **8** (1979) 329.
13) S. M. Butorin, J.-H. Guo, M. Magnuson and J. Nordgren: Phys. Rev. B **55** (1997) 4242.
14) From a quantitative point of view, the two-configuration approximation is poor one in the context of the large-N expansion theory [see, for a review, N. E. Bickers: Rev. Mod. Phys. **59** (1987) 845] because the number of degenerate orbitals is only two.
15) J. Zaanen, G. A. Sawatzky and J. W. Allen: Phys. Rev. Lett. **55** (1985) 418.
16) This is still true also for the larger value of $v = 3.5$ eV, which roughly simulates both e_g and t_{2g} orbitals.
17) J. Jiménez-Mier, J. van Ek, D. L. Ederer, T. A. Callcott, J. J. Jia, J. Carlisle, L. Terminello, A. Afsaw and R. C. Perera: Phys. Rev. B **59** (1999) 2649.
18) T. Minami: J. Phys. Soc. Jpn. **67** (1998) 3958; T. Minami and K. Nasu: J. Electron Spectrosc. Relat. Phenom. **92** (1998) 231.
19) G. van der Laan: Phys. Rev. B **41** (1990) 12366.
20) T. Higuchi, T. Tsukamoto, M. Watanabe, M. M. Grush, T. A. Callcott, P. C. Perera, D. L. Ederer, Y. Tokura, Y. Harada, Y. Tezuka and S. Shin: Phys. Rev. B **60** (1999) 7711.
21) Polarization dependence is another possible reason.
22) T. Minami and K. Nasu: Phys. Rev. B **57** (1998) 12084; T. Minami and K. Nasu: J. Electron Spectrosc. Relat. Phenom. **92** (1998) 213.